Linear shear rheology of aging β-casein films adsorbing at the air/water interface

F. Martínez-Pedrero[1,], J. Tajuelo[2], P. Sánchez-Puga[2], R. Chulia-Jordan[1], F. Ortega[1], M.A. Rubio[2], R. G. Rubio[1].*

[1]Departamento de Física-Química I, Universidad Complutense de Madrid, Avda. Complutense s/n, Madrid, 28040, Spain.

[2]Departamento de Física Fundamental, Universidad Nacional de Educación a Distancia, UNED, 28040 Madrid, Spain.

KEYWORDS. Shear Rheology, β-casein, microrheology.

ABSTRACT. In this work, the viscoelasticity of fragile β-casein films has been followed using different macro- and microrheological techniques. The modulus of the complex surface viscosity $|\eta^*|$ varies with time, allowing for the monitoring of the protein adsorption and annealing. β-casein adsorption creates a soft glassy gel at the interface that experiences an aging process. Macrorheological experiments with multiple probe sizes in addition to microrheological experiments demonstrated the consistency of the surface rheological properties over a broad range of viscosities. Surface pressure measurements were performed to complement the characterization of the processes.

1. Introduction

Interfacial rheology is the study of the mechanical response of the surface films to deformation. Interfacial shear and dilational rheology (ISR and IDR respectively) study constant area shape deformations and constant geometry compressions and expansions respectively[1]. The former is usually determined by measuring both the amplitude of the applied excitation and the linear or angular displacement of a probe placed on the interface, while the latter is usually determined from capillary wave experiments (surface light scattering or electrocapillary waves) or perturbing the internal pressure of bubbles or drops and measuring their shape changes. Since dilational and shear moduli correspond to distinct magnitudes which in principle are not correlated, interfacial shear and dilational rheology shed light on different aspects of the structure and dynamics of interfacial layers. In the literature, it is often assumed that the short-term stability of fluid dispersions is governed by dilatational magnitudes, whereas the long-term stability is mainly dictated by shear magnitudes[2]. However, most interfacial phenomena put into

play complex combinations of shear and dilational deformations, and this assumption is not always justified[3].

Even though the determination of the viscoelastic modulus is essential for the understanding of the physico-chemical mechanisms that govern interfacial processes, this is not straightforwardly accessible. In shear experiments, the induced motion of the probes is not only restricted by the resistance offered by the interfacial film, but also by the resistance exerted by the surrounding bulk phases. The decoupling of both responses is mandatory for understanding how the probe motion connects with the interfacial mechanical properties. In the preliminary studies, the ever-present bulk contribution was cancelled by subtracting the probe motion in an inviscid air-water interface from the response in the presence of the interfacial film. However, Verwijlen et al.[4] showed that at low Boussinesq number (Eq. 1),

$$Bo \equiv \frac{\eta_s P}{\eta A} \propto \frac{\eta_s}{\eta a} \ , \qquad (1)$$

this method leads to erroneous values of the dynamic surface moduli. Here η_s and η are the interfacial and bulk viscosities respectively, P the contact perimeter and A the wetted surface area of the probe[5]. For $Bo \ll 1$, the bulk contribution can be neglected and, consequently, the sensitivity of the interfacial rheometer increases. On the other hand, in the low Boussinesq number regime, the velocity profile at the interface is not linear. Therefore, it is necessary to assess the deformation profile in order to determine the surface mechanical properties. Since Bo is inversely proportional to the characteristic length a, which is linked to the probe size, the use of small probes leads to higher Bo values. This strategy, followed by different authors[6-10], allows for the measurement of surfaces viscosities in the order of 10^{-1}-10^{-9} Ns/m. In interfacial

microrheological techniques, the probe is only few microns in size, and the reduced size of the probes further increases the sensitivity of the method, allowing for the measurement of surface values of the order of 10^{-10} Ns/m[4, 11]. There exists in the literature a broad debate on the comparison of the values of the complex shear modulus measured with macro- with those measured with micro-rheological techniques[12]. This is a key issue because a complete understanding of the mechanical properties of interfacial films requires a coherent characterization at different length and time scales. Since viscoelasticity is an intrinsic material property, micro- and macro- techniques must agree in the range where both measurements are reliable.

Partially soluble proteins having roughly balanced segments, with hydrophilic and lipophilic tendencies, act as natural surfactants. The stabilization of dispersed systems by proteins is based on protein adsorption, interfacial unfolding, and the formation of viscoelastic networks[13-14]. The viscoelastic transition in protein layers has been frequently attributed to gel formation. However, other mechanisms resulting from repulsive non-covalent interactions have also been proposed[15]. Proteins adsorbed on an interface deform or even denature, depending on the degree of structural distortion. In contrast to small surfactant molecules, protein films are usually composed of an annealing multilayer structure. These structures are formed by denatured and native proteins, in most cases irreversibly adsorbed on the interface. Thus, the protein conformation on the interface does not only depend on thermodynamic magnitudes but also on adsorption time. The mechanism of the viscoelastic transition in protein layers is system-specific and determined by the characteristics of the continuous phases and by the protein species that come into play.

Shear rheological techniques provide useful information about different aspects of the adsorption process, the interactions between the proteins and the transient formation of the interfacial

layer[16]. In recent years, interfacial rheological techniques have become more sensitive and precise, providing significant new insight into protein arrangement on the surface layer. For example, the surface mechanical properties of albumin films at different aging times have been measured by monitoring the field-induced rotation of magnetic nanorods with a sensitivity comparable to that of passive microrheological techniques[17]. In dilatational rheology, the change in the area induced during the measurements implies changes in the surface concentration, and consequently can induce changes in the proportion of native and adsorbed proteins and in their structural conformation. In interfacial shear rheology, these problems do not arise since the measurements are performed at constant area[18-19]. It is generally accepted that globular proteins adsorb slower than random coil proteins, while the former eventually form more stable and stiffer networks[20-21]. Globular proteins form films that evolve with adsorption and aging from a fluid-like to a gel-like behaviour. When the proteins adsorb and unfold, the strong intramolecular interactions that stabilize the native conformation slowly turn into intermolecular interactions that stabilize the film. On the other hand, random coil proteins lack the capacity to form strong intermolecular bonds. They create much weaker films, physical gels or jammed states that barely change over time and where proteins arrange in loop-train conformations[22-24]. Globular proteins irreversibly bind to the interface whereas random-coil proteins can desorb into the bulk phase[18, 25-26].

The softness, instability and fragility of aging β-casein films adsorbing at the air/water interface call for the utilization of methods able to measure low viscoelastic modulus and, consequently, to mechanically characterize the adsorption mechanism. In this work, we use micro- and macro-rheological techniques to study the linear rheological evolution of those films. The magnetic rod interfacial shear rheometer used in our study[27] is able to measure viscoelastic modulus values

that are usually between those measured with micro- and macrorheological techniques. The use of these complementary methods may permit a complete characterization of the adsorption mechanism, providing new understanding of the interfacial mechanical changes occurring during the process.

2. Methods

a. Materials

Different batches of essentially salt-free lyophilized β-casein from bovine milk were purchased from Sigma Aldrich Co. (Germany). The purity of the applied protein sample, which determines its adsorption behavior[28], was always higher than 98%. The protein was stored at -18 °C and used without further purification. β-casein, the main surface active casein protein, is made up of 209 amino acids and has a molecular weight of 23.8 kDa. The entire molecule has an average hydrophobicity of 5.58 kJ, and presents an asymmetric configuration, with one third of all charged residues located within the first 50 amino acids of the N-terminal (the amine group of the first amino-acid). The remainder, the hydrophobic C-terminal (the carboxylic group of the last amino acid), is predominantly hydrophobic. All our measurements were performed at air/water interfaces, particularly relevant in the study of foam stability. At the air/water interface, protein adsorption, and eventual film reinforcement, are mainly determined by several factors: the flexibility and the linear character of β-casein, the protein concentration, and the absence of chemical bonds between the molecules. On the other hand, these properties are also largely affected by the temperature, pH and ionic strength of the aqueous phase. The aqueous subphase used in our experiments was a phosphate buffered saline (PBS) solution (Sigma Aldrich Co.) at

pH 7.4. Milli-Q purified water (resistivity higher than 14 MΩ·cm) was used for buffer preparation and all other purposes. In all our experiments, the dispersed proteins adsorb at freshly prepared interfaces. The batch solution was prepared daily by dissolving proper amounts of β-casein in 100 mL of phosphate buffer solutions having different ionic strengths, I = 0.10 M and 0.18 M. The buffer pH of 7.4, at which the proteins are negatively charged, is above the β-casein isoelectric point (4.5). It is worth mentioning that some authors describe significant differences between the dynamic properties of spread and adsorbed β-casein layers[26, 29-30].

b. Interfacial Rheology

Our study includes passive measurements, in which the Brownian motion of spherical colloidal particles at the interface is tracked, and active measurements, in which the forced translational motion of a magnetic needle at the interface is employed to infer layer rheology. The interfacial shear rheometer was developed in-house starting from the original design introduced by Shahin[31] and further developed by Brooks et al.[32], but the needle was driven with a magnetic tweezer configuration instead of classical Helmholtz coils[27]. To create the field gradient required to apply the magnetic force on the probe we employed a pair of small neodymium magnets, separated by a distance d and placed at a certain height h above the air/water interface. In the present study, the distance between the magnets was kept constant at d = 20 mm. We used two different probes. First, a commercial magnetic needle ISR28(KSV-NIMA), consisting of a hollow glass capillary of length 28.6 mm and outer diameter 400 μm, filled with an axially magnetized magnetic core of length 18.0 mm and diameter 270 μm (inset II in Figure 1). Second, a magnetic microwire of length 11.0 mm, outer diameter 24 μm, mass 0.024 mg, and a magnetization of (1.30 ± 0.04) 10^6A/m[7, 27] (inset III in Figure 1). Before each experiment, the surface pressure of the clean interface was measured to ensure the absence of surface-active contaminants in the solution,

obtaining values of between 0.0 and 0.3 mN/m. The surface tension of pure water at the temperature of the experiment, T = 22 ºC, was between 72.5 and 72.8 mN/m. In the time-dependent measurements, the probe position was monitored while the magnetic tweezers performed 15 periods of oscillation at a frequency of 0.25 Hz. Then, the amplitudes and the relative phase of the magnet pair and the probe oscillatory displacements were calculated using a Discrete Fourier Transform (DFT) procedure. The schematic of the device is shown in Fig 1, and a full description of the experimental set-up can be found in the reference[27].

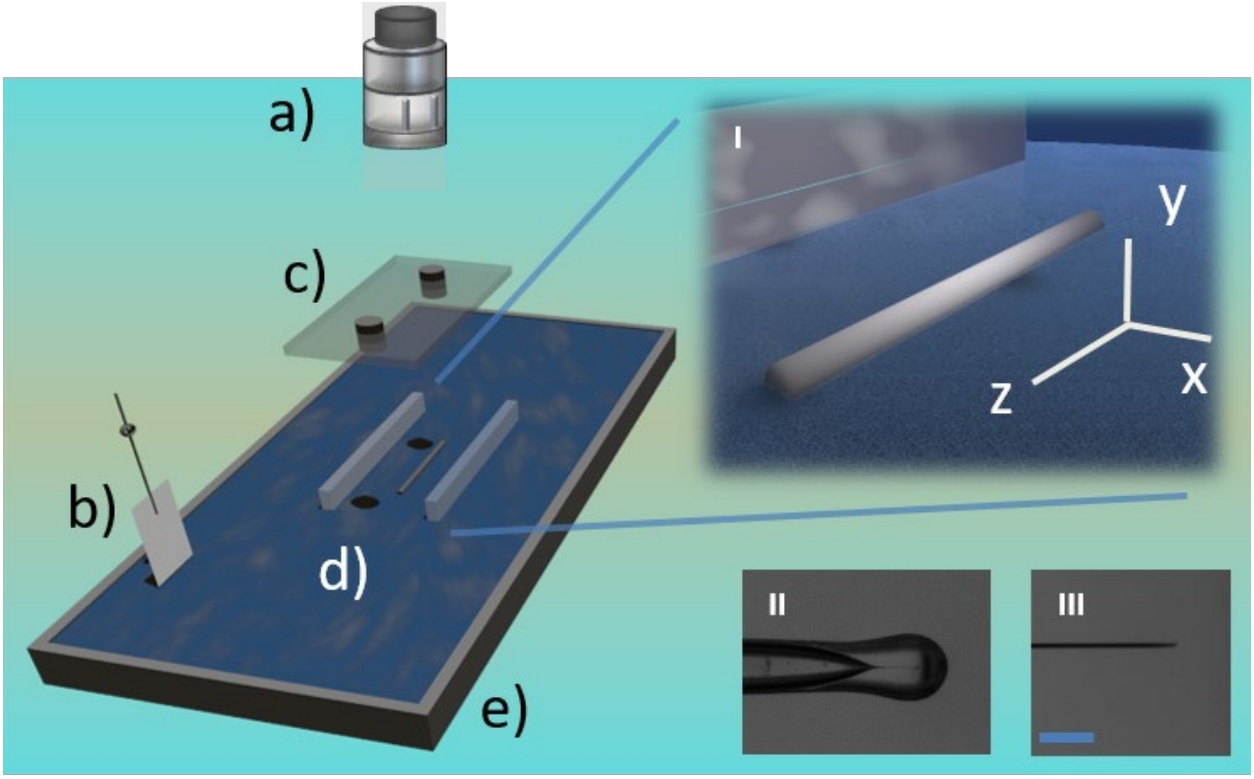

Figure 1 (color online): Schematic of the rheometer: a) Long working distance microscope and CCD camera. b). Surface tensiometer. c) Glass window and magnet pair, positioned by means of two precision linear stages (not shown) that are oriented along the z and y axes. d) Delrin channel and magnetic probe. e) Teflon Langmuir trough. The insets show: (I) a close-up view of the shear channel and the magnetic needle floating on the interface, together with the reference frame used

in the equations, (II) the commercial magnetic needle ISR28(KSV-NIMA), (III) and the magnetic microwire (scale bar is 300 μm).

Reynaert et al.[6] proposed a numerical scheme to solve the hydrodynamic equations of motion by means of a finite element Navier-Stokes solver in order to account for the effects of the underlying aqueous phase and to better interpret the experimental data. Later, Verwijlen et al. showed that the calculated velocity profile agreed with the profile measured from tracer microparticles adsorbed on the interface[4]. In addition, they proposed an iterative method to calculate Bo^* from the measured amplitude ratio. The iteration is repeated until convergence is achieved and a stable value of Bo^* is obtained. Once convergence is reached, the real (elastic G') and imaginary (dissipative G'') components of the complex viscoelastic modulus $G^* = G' + iG''$, and the complex viscosity are recovered by means of Eq.2:

$$\begin{aligned} G'(\omega) &= -\omega a \eta \,\mathrm{Im}\left[Bo^* \right] \\ G''(\omega) &= \omega a \eta \,\mathrm{Re}\left[Bo^* \right] \\ \eta_s^*(\omega) &= a \eta Bo^* \end{aligned} \quad , \qquad (2)$$

For the sake of completeness, we briefly outline here the procedure used to separate the subphase and surface contributions (a deeper description can be found in Tajuelo et al.[27]). First, we performed a calibration frequency sweep on a clean air-water interface before each measurement, keeping the vertical distance between the magnets and the needle constant. The resolution of the device is ultimately determined by the capability of measuring the small differences between the response when the probe is dragged on the surfactant-laden interface and the clean water interface. The force balance equation of the probe, considering the subphase and surface contributions, is given by:[6]

$$\frac{F_0 e^{i\omega t}}{z_0^* e^{i\omega t}} = i2L\omega\eta \cdot Bo^* \left(-\frac{\partial g^*}{\partial p} \right)\Bigg|_{p=0,\theta=\pi/2} + i2L\omega\eta \int_0^{\pi/2} -\left(\frac{\partial g^*}{\partial p} \right)\Bigg|_{p=0} d\theta + k - m\omega^2 , \quad (3)$$

where F_0 is the amplitude of the oscillatory force, acting on the probe with a frequency ω, z_0 is the amplitude of the probe displacement, L is the probe length, $g^*(p)$ is the velocity field profile, and $p = ln(r/a)$ is the non-dimensional radial coordinate. Here a is the probe radius and r the radial distance between the axis of the probe and the fluid element. The first and second terms on the right-hand side of Eq. 3 represent, respectively, the surface and subphase drag. k is the system compliance that arises from the small elastic force, usually imposed on the probe to keep it in place by either magnetic coils[6] or a small permanent magnet[7]. The fourth term is an inertia term where m is the probe mass. Interestingly, Tajuelo et al. showed how the substitution of magnetic coils by a magnet pair trap makes the value of k in Equation 3 strictly zero. They also showed that the resolution of the instrument with the magnetic needles is around $3 \cdot 10^{-8}$ Ns/m, and goes down to $3 \cdot 10^{-9}$ Ns/m with the microwire probes. Therefore, the micrometric dimension of the microwire provides a sensitivity close to that measured by passive microrheological techniques. Compared to the passive microrheological methods, a microwire enables measurement in more viscous films.

c. Passive Microrheology

In the micro-rheology experiments we used negatively charged surfactant-free polystyrene microparticles (1.0 μm diameter) having sulfate functional groups at their surface yielding a surface charge density $C \approx$ - 6 μC/cm^2 (Molecular Probes, Interfacial Dynamics Corporation, USA). They were dispersed in 50% v/v water/2-propanol (IPA, 99%, Sigma-Aldrich), and a 50 μl droplet of the dispersion was injected in the aqueous phase, close to the surface. In principle,

the 2-propanol present in the spreading solution might affect layer formation at the interface. However, previous studies performed with lysozyme solutions showed that IPA did not have a significant influence on the interface's rheological properties[33]. All the microrheological experiments were performed on a Newport vibration isolation table, in a temperature controlled well with a temperature stability better than 0.1 ºC, with water on the bottom and air on the top half. Random flow currents at the interface were minimized by covering the cell with a transparent slide cover and by keeping the temperature constant at T = 22 ºC with a thermostated circulation bath. Before each experiment, the sample cell was cleaned thoroughly by scrubbing with Alconox soap solution and IPA and then rinsed repeatedly in deionized water. The colloids at the interface were monitored by using an inverted bright-field microscope (Nikon Eclipse 80-I microscope) with a x50 objective (WD 2.7-3.7 mm, NA 0.6). A video camera (Nikon D3100) recorded at a rate of 30 frames per second, a speed that sets the shortest time t = 0.033 s over which the probe trajectory can be followed. In our analysis, we only monitored those isolated particles that presented a slower diffusion. Hence, we tracked the particles confined on the interface and not in the near-surface subphase[34-35]. The relative mean square displacement of the particles located within the field of view was calculated using:

$$MSD_{rel} = \left\langle \Delta r_{rel}^2(\tau) \right\rangle = \left\langle (\Delta \vec{r}_{ij}(t+\tau) - \Delta \vec{r}_{ij}(t))^2 \right\rangle . \qquad (4)$$

The above averages were taken over all the pairs of particles *i* and *j*, and initial times, *t*, of the process. The drift of the particles was partially eliminated from the analysis by subtracting the average velocity of the ensemble from that of each particle. The need for distinguishing Brownian particle displacements from others types of experimental fluctuations, such as, for instance, ambient vibration or thermal noise of the camera, limits the applicability of this technique to weak films. The relative mean square displacement is twice the mean square

displacement (MSD) $\left\langle \Delta\tilde{r}_{rel}^{\,2}(\tau)\right\rangle = 2\left\langle \Delta\tilde{r}^{2}(\tau)\right\rangle$. The former was finally corrected by subtracting the asymptotic value of the mean squared displacement at short times[36], which is usually assigned to the square amplitude of the ambient vibrations. The MSD is related to the complex viscoelastic modulus through the Generalized Stokes-Einstein (GSE) equation

$$\left\langle \Delta\tilde{r}^{2}(\nu)\right\rangle = \frac{2k_B T}{3\pi a \nu \tilde{G}(\nu)}, \qquad (5)$$

first proposed ad-hoc by Mason and Weitz[37], and later rigorously proved by Levine and Lubensky[38]. Here, $\left\langle \Delta\tilde{r}^{2}(\nu)\right\rangle$ and $\tilde{G}(\nu)$ are the Laplace transforms of the mean square displacement and the stress relaxation modulus, where ν is the Laplace frequency. This equation is only valid when the size of the particle is larger than any spatial heterogeneity of the material. Mason used methods based on local power-law approximations of the mean square displacement to obtain algebraic expressions able to estimate the viscoelastic moduli as a function of the angular frequency ω

$$\left|G^{*}(\omega)\right| \approx \frac{k_B T}{\pi a \left\langle \Delta r^{2}(1/\omega)\right\rangle \Gamma\left[1+\kappa(\omega)\right]}, \qquad (6)$$

where Γ is the gamma function and $\kappa(\omega) \equiv \left.\frac{d\ln\left\langle \Delta r^{2}(t)\right\rangle}{d\ln t}\right|_{t=1/\omega}$[39]. We used Eq. 6 to calculate the viscoelastic modulus from the tracked position of the particles.

3. Experimental Results

    a. Magnetic microwire measurements

Using the interfacial shear rheometer, we characterized the adsorption of β-casein by monitoring the change of Π, $|\eta_s^*|$, and the dynamic moduli G' and G'', keeping the interfacial area and the temperature T = 22 ºC constant. These magnitudes depend on the amount and configuration of adsorbed proteins and, thus, they allowed us to gain insight on the adsorption process. In Figure 2 we show two experiments performed at ν = 0.25 Hz, I = 100 mM, and two different bulk concentrations, ρ = 1.4 10^{-4} wt% and ρ = 5.5 10^{-3} wt%.

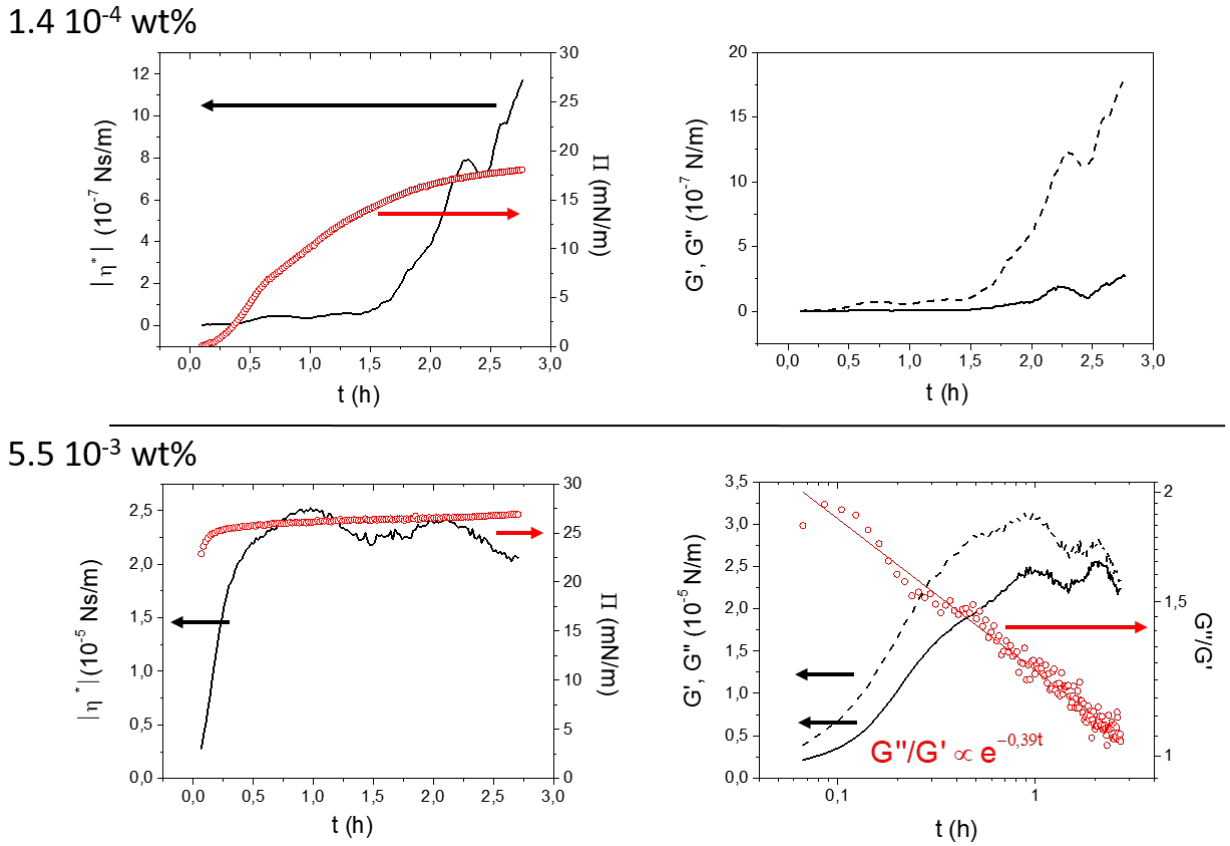

Figure 2 (color online): Time evolution of $|\eta_s^*|$ (black line), Π (red circles) (left column), G' (black continuous line), G'' (black dashed line) and G''/G' (red circles) (right column), measured on the "freshly prepared" air/β-casein aqueous solution interface. Experimental parameters were ν = 0.25 Hz, I = 100 Mm, and two bulk concentrations, ρ = 1.4 10^{-4} wt% (upper row) and ρ = 5.5

10^{-3} wt% (bottom row). In the latter concentration, the ratio between the viscous and the elastic moduli follows a power-law trend $G''/G' \propto e^{-0.39t}$.

In the most diluted solution, the surface pressure increased with time, starting from 0.0 mN/m to approximately 17.5 mN/m. The continuous increase of the surface pressure can be explained by the ongoing adsorption of the proteins at the air/water interface. Once adsorbed on the interface, the hydrophilic block of the β-casein, the N-terminal, goes into the aqueous phase whereas the hydrophobic C-terminal spreads on the non-polar phase. The evolution of the surface pressure is faster than that described by common diffusion models, as discussed in[40-41]. The surface viscosity was low for the first 90 minutes but increased by one order of magnitude in one hour when the surface pressure was above 15mN/m. At relatively high surface pressure the β-casein molecules adsorbed on the interface form a viscous physical gel, a cross-linked structure promoted by hydrophobic or steric interactions, made up of aggregates large enough to affect rheological measurements[30]. In the right column, we show how this increase is mostly due to the viscous modulus, which was higher than the elastic modulus for the whole measurement range. At the highest bulk concentration $\rho = 5.5\ 10^{-3}$ wt%, the surface pressure initially increased very quickly to a value of approximately 22.5 mN/m, and then reached a plateau that slightly increased over time periods longer than one hour. Usually, this slow increase is interpreted in terms of conformational changes in proteins[23]. In contrast to the previous continuous increase in the surface pressure, the surface viscosity presented two faint maxima, after 45 and 120 minutes respectively, at values much higher than those measured in the diluted solution. The first decrease, accompanied by an increase of the surface pressure, was also detected in dilational measurements when the concentration or surface pressure was increased, and is usually explained by the displacement of the hydrophilic N-terminals into the aqueous phase, where they

form tails and loops. Cicuta et al. proposed that the proteins only formed loops in the range of a second maximum[42]. However, the presence of loops around the first maximum has been confirmed by neutron reflectivity[43]. This first maximum has also been explained in terms of the Vroman effect, a competitive adsorption and unfolding of native and denatured proteins, primarily described for protein adsorption at solid surfaces but that has been also observed at liquid interfaces[18]. The increase of the complex interfacial viscosity up to the second local maximum was slightly smaller than the first, and in the dilatational measurements it is usually explained by the interaction between the most hydrophobic parts of the proteins, which are displaced into the aqueous phase at high surface pressures. After the second maximum, the β-casein molecules adopt a more compact intermolecular conformation, with a reduced interfacial mass density, that leads to the final decrease in surface shear visco-elasticity. To explain the appearance of a second maximum, other authors consider also the possibility of the formation of a second protein layer[29, 44]. The dangling tail model, that describes the film as a non-homogeneous distribution of proteins in a two-layer structure, better explains the results obtained in neutron reflectivity[18, 43, 45]. Real interfaces are regions of a certain thickness and this fact hampers the interpretation of the results[46]. As we show in the right column in Figure 3, the global response of the dense monolayer is mainly driven by the viscous component but the loss tangent G''/G' starts to shrink before reaching the first maximum, following a power-law dependence $G''/G' \propto e^{-0.39t}$. The simultaneous increase of elasticity and decrease of viscosity is related to the stability of protein foams and/or emulsions[14, 47]. In summary, at high protein concentrations non-covalent interactions between the adsorbed proteins induce the formation of cross-linked structures that relax through spatial rearrangements and, probably, the creation of a multilayer.

The specific behaviors shown in Figure 2 are not quantitatively reproducible since the time evolution of the viscoelastic modulus slightly depends on the experimental realization. There are various reasons that could explain the reduced reproducibility. At bulk concentrations lower than $\rho = 1.0\ 10^{-3}$ wt%, uncontrolled protein adsorption on the glass surface of the volumetric flask where the sample is prepared, or on the surface of the Teflon Langmuir trough, may significantly change the experimental bulk concentration and consequently the adsorption rate, as pointed out by Bantchev et al.[24]. On the other hand, the probe positioning process can disrupt the monolayer formed during the initial steps of protein adsorption. This history-dependence highlights the caution required in interpreting the results of dynamic measurements on these monolayers. Figure 3.a shows the change in surface viscosity over time, measured at 4 different bulk concentrations, and averaged over 3 experiments.

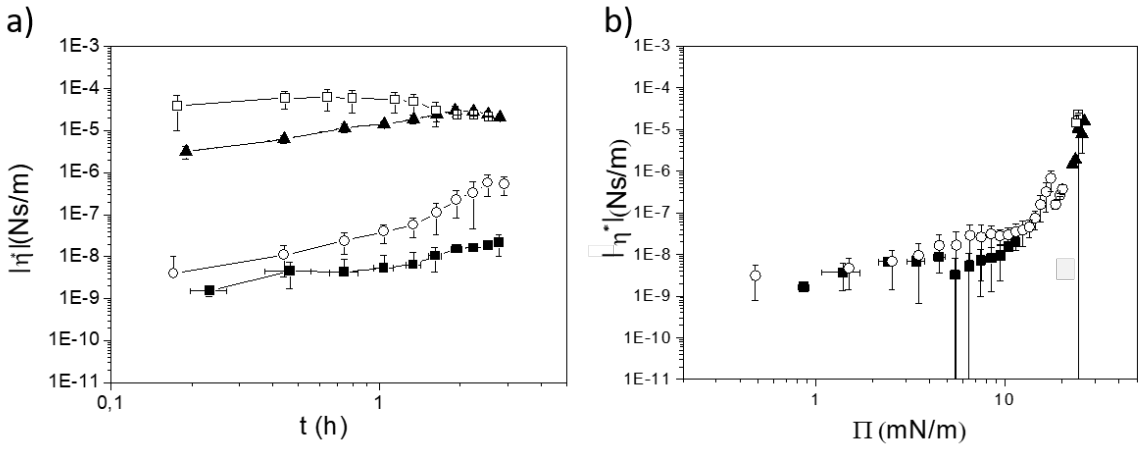

Figure 3: The modulus of the average complex surface viscosity $|\eta_s^*|$ as a function of the adsorption time (a), and the surface pressure (b), at 4 different concentrations: $\rho = 2.0\ 10^{-5}$ wt% (filled squares), $\rho = 1.4\ 10^{-4}$ wt% (circles), $\rho = 1.1\ 10^{-3}$ wt% (triangles), and $\rho = 5.5\ 10^{-3}$ wt% (empty squares).

Using the ISR28 magnetic needle and the microwire, we made precise measurements over five decades in complex viscosity. We found that bulk concentrations approximately between $\rho = 2.0\ 10^{-5}$ wt% and $\rho = 5.0\ 10^{-3}$ wt% had a measurable surface shear viscosity. At low concentrations, the modulus of complex viscosity monotonously increased with the adsorption time. The higher the protein concentration the faster was the adsorption. Thus, the equilibrium was only quickly reached for the most concentrated bulk solution of $\rho = 5.5\ 10^{-3}$ wt%. At this concentration, the molecules arrange in a compact intermolecular conformation, which leads to a posterior decrease in surface shear viscosity[48]. For all the bulk concentrations and adsorption times explored, G' was found to be lower than G'', so that at this frequency the β-casein monolayer was predominantly viscous. The discrepancy of roughly three orders of magnitude with the values reported in reference 24 is due, most probably, to the intrinsic limitations of the Helmholtz coil interfacial rheometer when high inertia probes and a linear subtraction of the subphase contribution are used (techniques based on the flow field for subphase drag subtraction were developed several years later; see Refs. 6, 7, 27). In Figure 3.b we plot the modulus of the complex surface viscosity as a function of the surface pressure, measured over time for all the β-casein bulk concentrations. Measurements suggest that the first rheological changes, related to thickening or gelation, are observed when the surface pressure is higher than 10 mN/m. For flexible proteins, such as caseins, the dependence of the surface viscosity on the surface pressure is much more marked than for globular proteins. Here, the surface pressure varies by three orders of magnitude in the range of between 10 and 25 mN/m. This approximated trend is also much more pronounced than those previously reported for PtBMA, hexadecanol, and DPPC[12]. Above 10 mN/m, the hydrophobic and steric interactions between the adsorbed proteins promote cross-linked structures which can dramatically increase the viscoelastic response of the films[21].

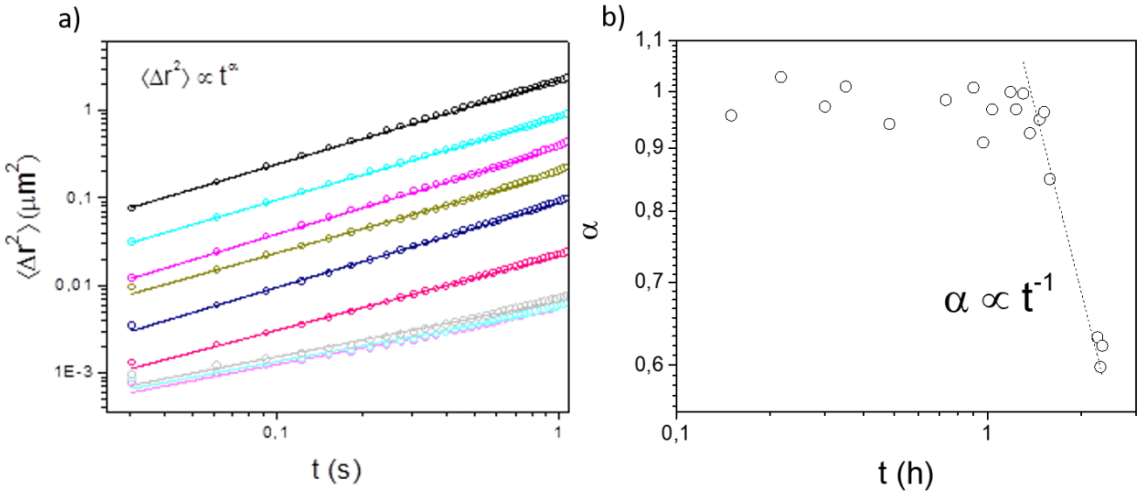

Figure 4 (color online): (a) Ensemble-average relative mean-squared displacements of 0.5 μm radius colloids at the air/ β-casein aqueous solution (ρ = 1.4 10^{-4} wt%, pH = 7.4) at (top down) 8 (black), 30 (cyan), 45 (magenta), 54 (dark yellow), 60 (navy blue), 90 (pink), 130 (grey), 135 (light cyan), 140 (light magenta) minutes after formation of the interface. The solid lines are the results of power-law fits $\left\langle \Delta r^2(\tau) \right\rangle \propto t^{\alpha}$. (b) The power-law exponent α as a function of aging time for the same protein concentration. After gelation, this magnitude follows a power-law trend with t, $\alpha \propto t^{-1}$, represented by the dashed straight line.

b. Comparison between the macro- and the microrheological measurements

Figure 4.a shows how the formation of the β-casein film affects the diffusive motion of colloids at the air/water interface of the β-casein solution, for a bulk concentration of ρ = 1.4 10^{-4} wt%, as a function of age after the formation of the interface. The microrheological measurements are restricted to low bulk concentrations since thermal fluctuations only allow the characterization of relatively weak films. As expected, the gradual adsorption of the proteins at the interface constrained the motion of the particles from a diffusive to a subdiffusive behavior. At the longest measured times, Brownian diffusion of the particles was almost qualitatively imperceptible,

being the drift the dominant motion. As explained in the Methods section, the influence of the ambient vibration on the analysis of the measurements was corrected by subtracting the extrapolated mean square displacement at t = 0 from all the measurements. Figure 4.b shows the power-law exponent α, characterizing the mean-squared displacement time dependence $\left\langle \Delta r^2(\tau) \right\rangle \propto t^{\alpha}$, for different aging times of protein adsorption. Initially, α = 1 and the film was strictly viscous, but after approximately 90 minutes the power-law exponent decreased approximately as t^{-1} and the film became viscoelastic, with α = (0.60 ± 0.03) in the latest measurements.

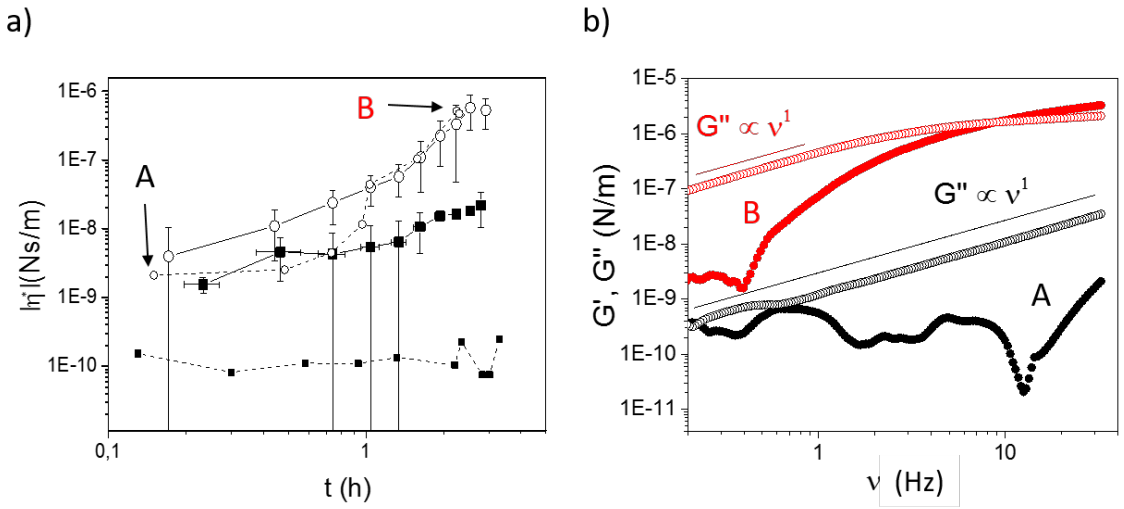

Figure 5 (color online): (a) Modulus of the complex surface viscosity, measured with ISR (large symbols) and particle tracking (small symbols) at a frequency of 0.25 Hz, for two different bulk concentrations, ρ = 2.0 10^{-5} wt% (filled squares) and ρ = 1.4 10^{-4} wt% (circles). (b) The interfacial dynamic moduli as a function of frequency measured with particle tracking, 8 and 130 minutes after the formation of the interface, corresponding to points A and B in Figure 5.a. Here, the filled circles represent the elastic modulus, the empty circles the viscous modulus, and the concentration of the β-casein solution was ρ = 1.4 10^{-4} wt%.

In Figure 5.a, we compare the macro- and microrheological measurements for the two most dilute solutions. The differences observed in the most diluted sample could be due to the lack of sensitivity of the ISR (interfacial complex viscosities lower than 10^{-9} N/m), which is unable to provide reliable data at such low interfacial density even when the microwire probe is used. These differences could also be due to the inherent differences found in the literature between the passive and the active interfacial methods [49]. At the highest bulk concentration, $\rho = 1.4\ 10^{-4}$ wt%, the values of the complex surface viscosity measured using the microwire probes almost superpose those measured with particle tracking. The quantitative agreement between the microrheological and the ISR measurements in the most concentrated solutions, at least for the latter range of values, validates the quantitative capabilities of the micro-probe for measuring weak films of soluble proteins. For viscous modulus higher than $3 \cdot 10^{-9}$ Ns/m, a value that is roughly equal to the resolution of the rheometer, the results obtained with both techniques almost coincide. Another way to look at the variation of the mechanical properties of the films is shown in Figure 5.b, where we represent the microrheological measurements of G' and G'' versus frequency for "freshly prepared" and aged monolayers, in suspensions with a bulk concentration of $\rho = 1.4\ 10^{-4}$ wt%. In the curves corresponding to the point A, G'' exhibits a linear dependence on frequency $G'' \propto \nu$, whereas G' is found to be noisy and negligible when compared to G''. Hence, the β-casein monolayer is predominantly viscous independently of the frequency. In the aged film (curves B), the dynamic moduli are at least two orders of magnitude larger. The linear dependence of G'' over viscous behavior is still observed at low frequencies, reaching a plateau at frequencies around 5 Hz. At 8 Hz there is a crossover after which $G'' \leq G'$, indicating that the monolayer stores elastic energy for time scales above 0.1 s. At long aging times and high enough concentrations, β-casein creates films like those formed by globular proteins, where the elastic

interfacial modulus is higher than the viscous component[20, 23]. There is still no unanimity on the quantitative rheological criteria for gelation; for some authors the gelation criterion is the appearance of non-zero shear elasticity, other authors propose G' > G'' for all frequencies while others G' > G'' with aging, independently on the frequency. Anyway, Fig. 5b shows that the adsorbed proteins evolve from a pure viscous layer to a stiffer viscoelastic film. This result contradicts previous studies which stated that the β-casein adsorbed monolayers remain fluid at all concentrations[50].

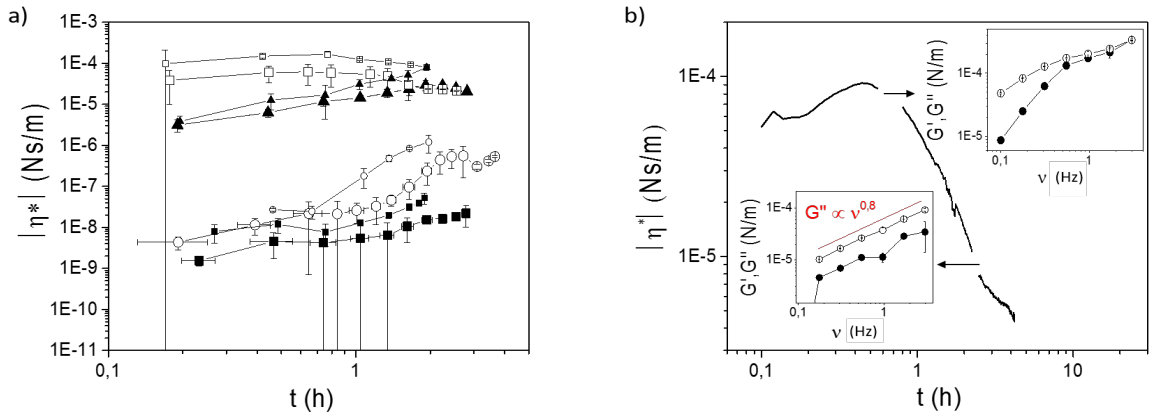

Figure 6 (color online): (a) Change in the average modulus of the complex surface viscosity measured with ISR over time, at I = 180 mM (small symbols), for 4 different concentrations: ρ = 2.0 10-5 wt% (filled squares), ρ = 1.4 10^{-4} wt% (circles), ρ = 1.1 10^{-3} wt% (triangles) and ρ = 5.5 10^{-3} wt% (empty squares). The values are compared with the results obtained for I = 100 mM (large symbols). (b) Change in the modulus of the complex surface viscosity $|\eta_s^*|$ over time, measured on the "freshly prepared" air/ β-casein aqueous solution, for ν = 0.25 Hz, I = 180 Mm and ρ = 5.5 10^{-3} wt%. The insets show the dynamic moduli versus frequency of the aged films after 40 and 130 minutes.

c. Effect of ionic strength

Figure 6.a compares the modulus of the complex viscosity as a function of aging time, for samples prepared at two different ionic strengths, I = 100 mM (big symbols) and I = 188mM (small symbols). The increase in the ionic strength screens the electrostatic interaction between the proteins. Therefore, even if the films prepared at relatively high ionic strengths were stiffer, the observed trends were similar. Again, in the most diluted samples, the modulus of the complex viscosity monotonously increased with the adsorption time, whereas in the most concentrated suspension, we first detected a maximum and then a subsequent decrease in the surface shear viscosity. Figure 6.b shows a specific measurement performed at 0.25 Hz for a bulk monolayer of $\rho = 5.5\ 10^{-3}$ wt%. We observed a maximum in the modulus of the complex interfacial shear viscosity followed by a decrease linked to changes in the structural conformation of the adsorbed proteins. We measured the viscoelastic modulus as a function of the frequency, just after detecting the maximum, and 2 hours later. In both cases, the viscous modulus was higher than the elastic modulus and the film evolved towards a softer conformation, where the viscous modulus G'' exhibits a power-law dependence on frequency $G'' \propto \nu^{0.8}$. In summary, the screening of the electrostatic repulsion, induced by the increase in ionic strength, did not qualitatively change the mechanical behavior of the films. The films formed at the same protein bulk concentration presented similar behavior over time and viscous behavior at relatively low frequencies, regardless of the ionic strength. Those films formed at higher ionic strength, however, were quantitatively stiffer.

4. Conclusions

In this work, we have characterized the adsorption process of β-casein on a bare air-water interface through the evolution of surface pressure and interfacial dynamic moduli, measured with macro- (ISR) and micro- (particle tracking) rheological techniques. In contrast to the

continuous increase measured in the surface pressure, the modulus of the surface complex viscosity was initially negligible and then, for a surface pressure of 10 to 15 mN/m, it suddenly increased with the adsorption time, in a thickening process mainly driven by the viscous component. At high enough bulk concentrations, however, the modulus of the complex viscosity presented one or two maxima. These maxima resemble those measured in dilational measurements, that are usually interpreted in terms of configurational transitions within the protein film and the formation of a second protein layer. The viscous monolayer evolves into a stiffer viscoelastic film that stores elastic energy over 0.1 s time scales. At higher ionic strengths, the films became stiffer but the observed mechanical behavior was qualitatively analogous. The methods used here, non-equilibrium rheological measurements performed with the recently developed magnetic trap interfacial shear rheometer, and equilibrium measurements using particle tracking, provide the most sensitive and precise mechanical characterization of the β-casein adsorption to date[2, 24, 50]. The quantitative agreement between the micro and the macrorheological measurements validates the approximations adopted in the microrheological methods and the quantitative capabilities of both techniques for measuring subtle and unstable protein films.

AUTHOR INFORMATION

Corresponding Author

***(fernandm@ucm.es)**

Author Contributions

All authors have given approval to the final version of the manuscript.

Funding Sources

Spanish Ministry of Economy and Competitiveness and the European Union.

ACKNOWLEDGMENT

F.M.P. acknowledges support from MINECO (Grant No. RYC-2015-18495). J.T. acknowledges a grant from UNEDs Researchers Formation Program. P.S.P. acknowledges a grant from Comunidad de Madrid. M.A.R and P.S.P. acknowledge partial support from MINECO (Grant No. FIS2013-47350-C5-5-R). F.O. and R.G.R. acknowledge partial support from MINECO (GrantsCTQ2016-78895-R and FIS2014-62005-EXP) and from E.U. through ITN Cowet. We also acknowledge Juan Manuel Pastor for fruitful discussions, and Manuel Vázquez for supplying the magnetic microwires.

REFERENCES

1. Mendoza, A. J.; Guzman, E.; Martinez-Pedrero, F.; Ritacco, H.; Rubio, R. G.; Ortega, F.; Starov, V. M.; Miller, R., Particle Laden Fluid Interfaces: Dynamics and Interfacial Rheology. *Advances in colloid and interface science* **2014**, *206*, 303-19.

2. Patino, J. M.; Sanchez, C. C., Structural, Topographical, and Shear Characteristics of Milk Protein and Monoglyceride Monolayers Spread at the Air-Water Interface. *Langmuir : the ACS journal of surfaces and colloids* **2004**, *20*, 4530-9.

3. Blijdenstein, T. B. J.; de Groot, P. W. N.; Stoyanov, S. D., On the Link between Foam Coarsening and Surface Rheology: Why Hydrophobins Are So Different. *Soft Matter* **2010**, *6*, 1799-1808.

4. Verwijlen, T.; Moldenaers, P.; Stone, H. A.; Vermant, J., Study of the Flow Field in the Magnetic Rod Interfacial Stress Rheometer. *Langmuir : the ACS journal of surfaces and colloids* **2011**, *27*, 9345-9358.

5. Butterworth-Heinemann Series in Chemical Engineering A2 - Edwards, David A. In *Interfacial Transport Processes and Rheology*, Brenner, H.; Wasan, D. T., Eds. Butterworth-Heinemann: Boston, 1991; p ii.

6. Reynaert, S.; Brooks, C. F.; Moldenaers, P.; Vermant, J.; Fuller, G. G., Analysis of the Magnetic Rod Interfacial Stress Rheometer. *Journal of Rheology* **2008**, *52*, 261-285.

7. Tajuelo, J.; Pastor, J. M.; Martinez-Pedrero, F.; Vazquez, M.; Ortega, F.; Rubio, R. G.; Rubio, M. A., Magnetic Microwire Probes for the Magnetic Rod Interfacial Stress Rheometer. *Langmuir : the ACS journal of surfaces and colloids* **2015**, *31*, 1410-1420.

8. Anguelouch, A.; Leheny, R. L.; Reich, D. H., Application of Ferromagnetic Nanowires to Interfacial Microrheology. *Appl. Phys. Lett.* **2006**, *89*, 3.

9. Kim, K.; Choi, S. Q.; Zasadzinski, J. A.; Squires, T. M., Interfacial Microrheology of Dppc Monolayers at the Air-Water Interface. *Soft Matter* **2011**, *7*, 7782-7789.

10. Zell, Z. A.; Mansard, V.; Wright, J.; Kim, K.; Choi, S. Q.; Squires, T. M., Linear and Nonlinear Microrheometry of Small Samples and Interfaces Using Microfabricated Probes. *Journal of Rheology* **2016**, *60*, 141-159.

11. Dhar, P.; Fischer, T. M.; Wang, Y.; Mallouk, T. E.; Paxton, W. F.; Sen, A., Autonomously Moving Nanorods at a Viscous Interface. *Nano letters* **2006**, *6*, 66-72.

12. Samaniuk, J. R.; Vermant, J., Micro and Macrorheology at Fluid-Fluid Interfaces. *Soft Matter* **2014**, *10*, 7023-7033.

13. Dickinson, E., Interfacial Particles in Food Emulsions and Foams. In *Colloidal Particles at Liquid Interfaces*, Binks, B. P.; Horozov, T. S., Eds. Cambridge University Press: Cambridge, 2006; pp 298-327.

14. Maldonado-Valderrama, J.; Martín-Rodriguez, A.; Gálvez-Ruiz, M. J.; Miller, R.; Langevin, D.; Cabrerizo-Vílchez, M. A., Foams and Emulsions of B-Casein Examined by Interfacial Rheology. *Colloids and Surfaces A: Physicochemical and Engineering Aspects* **2008**, *323*, 116-122.

15. Quinn, G.; Monahan, F. J.; O'Riordan, E. D.; O'Sullivan, M.; Longares, A., Role of Covalent and Noncovalent Interactions in the Formation of Films from Unheated Whey Protein Solutions Following Ph Adjustment. *Journal of Food Science* **2003**, *68*, 2284-2288.

16. Maldonado-Valderrama, J.; Patino, J. M. R., Interfacial Rheology of Protein–Surfactant Mixtures. *Current Opinion in Colloid & Interface Science* **2010**, *15*, 271-282.

17. Dhar, P.; Cao, Y. Y.; Fischer, T. M.; Zasadzinski, J. A., Active Interfacial Shear Microrheology of Aging Protein Films. *Physical review letters* **2010**, *104*, 4.

18. Mezzenga, R.; Fischer, P., The Self-Assembly, Aggregation and Phase Transitions of Food Protein Systems in One, Two and Three Dimensions. *Rep. Prog. Phys.* **2013**, *76*, 43.

19. Krägel, J.; Derkatch, S. R., Interfacial Shear Rheology. *Current Opinion in Colloid & Interface Science* **2010**, *15*, 246-255.

20. Freer, E. M.; Yim, K. S.; Fuller, G. G.; Radke, C. J., Interfacial Rheology of Globular and Flexible Proteins at the Hexadecane/Water Interface: Comparison of Shear and Dilatation Deformation. *The Journal of Physical Chemistry B* **2004**, *108*, 3835-3844.

21. Mitropoulos, V.; Mutze, A.; Fischer, P., Mechanical Properties of Protein Adsorption Layers at the Air/Water and Oil/Water Interface: A Comparison in Light of the Thermodynamical Stability of Proteins. *Advances in colloid and interface science* **2014**, *206*, 195-206.

22. Graham, D. E.; Phillips, M. C., Proteins at Liquid Interfaces .5. Shear Properties. *J. Colloid Interface Sci.* **1980**, *76*, 240-250.

23. Freer, E. M.; Yim, K. S.; Fuller, G. G.; Radke, C. J., Shear and Dilatational Relaxation Mechanisms of Globular and Flexible Proteins at the Hexadecane/Water Interface. *Langmuir : the ACS journal of surfaces and colloids* **2004**, *20*, 10159-10167.

24. Bantchev, G. B.; Schwartz, D. K., Surface Shear Rheology of Beta-Casein Layers at the Air/Solution Interface: Formation of a Two-Dimensional Physical Gel. *Langmuir : the ACS journal of surfaces and colloids* **2003**, *19*, 2673-2682.

25. Dickinson, E., Proteins at Interfaces and in Emulsions - Stability, Rheology and Interactions. *J. Chem. Soc.-Faraday Trans.* **1998**, *94*, 1657-1669.

26. Maldonado-Valderrama, J.; Wege, H. A.; Rodríguez-Valverde, M. A.; Gálvez-Ruiz, M. J.; Cabrerizo-Vílchez, M. A., Comparative Study of Adsorbed and Spread B-Casein Monolayers at the Water−Air Interface with the Pendant Drop Technique. *Langmuir : the ACS journal of surfaces and colloids* **2003**, *19*, 8436-8442.

27. Tajuelo, J.; Pastor, J. M.; Rubio, M. A., A Magnetic Rod Interfacial Shear Rheometer Driven by a Mobile Magnetic Trap. *Journal of Rheology* **2016**, *60*, 1095-1113.

28. Erni, P.; Fischer, P.; Windhab, E. J.; Kusnezov, V.; Stettin, H.; Lauger, J., Stress- and Strain-Controlled Measurements of Interfacial Shear Viscosity and Viscoelasticity at Liquid/Liquid and Gas/Liquid Interfaces. *Rev. Sci. Instrum.* **2003**, *74*, 4916-4924.

29. Noskov, B. A., Protein Conformational Transitions at the Liquid-Gas Interface as Studied by Dilational Surface Rheology. *Advances in colloid and interface science* **2014**, *206*, 222-238.

30. Noskov, B. A.; Latnikova, A. V.; Lin, S. Y.; Loglio, G.; Miller, R., Dynamic Surface Elasticity of Beta-Casein Solutions During Adsorption. *J. Phys. Chem. C* **2007**, *111*, 16895-16901.

31. Shahin, G. T. The Stress Deformation Interfacial Rheometer. University of Pennsylvania, 1986.

32. Brooks, C. F.; Fuller, G. G.; Frank, C. W.; Robertson, C. R., An Interfacial Stress Rheometer to Study Rheological Transitions in Monolayers at the Air−Water Interface. *Langmuir : the ACS journal of surfaces and colloids* **1999**, *15*, 2450-2459.

33. Allan, D. B.; Firester, D. M.; Allard, V. P.; Reich, D. H.; Stebe, K. J.; Leheny, R. L., Linear and Nonlinear Microrheology of Lysozyme Layers Forming at the Air-Water Interface. *Soft Matter* **2014**, *10*, 7051-7060.

34. Schuker, H., *Kolloid-Z* **1967**, *380*, 216.

35. Sheppard, E.; Tcheurekdjian, N., *J. Colloid Interface Sci.* **1968**, *28*, 481.

36. Waigh, T. A., Advances in the Microrheology of Complex Fluids. *Rep. Prog. Phys.* **2016**, *79*, 62.

37. Mason, T. G.; Weitz, D. A., Optical Measurements of Frequency-Dependent Linear Viscoelastic Moduli of Complex Fluids. *Physical review letters* **1995**, *74*, 1250-1253.

38. Levine, A. J.; Lubensky, T. C., One- and Two-Particle Microrheology. *Physical review letters* **2000**, *85*, 1774-1777.

39. Mason, T. G., Estimating the Viscoelastic Moduli of Complex Fluids Using the Generalized Stokes–Einstein Equation. *Rheologica Acta* **2000**, *39*, 371-378.

40. Miller, R.; Kragel, J.; Wustneck, R.; Wilde, P. J.; Li, J. B.; Fainerman, V. B.; Loglio, G.; Neumann, A. W., Adsorption Kinetics and Rheological Properties of Food Proteins at Air/Water and Oil/Water Interfaces. *Nahr.-Food* **1998**, *42*, 225-228.

41. Wüstneck, R.; Krägel, J.; Miller, R.; Fainerman, V. B.; Wilde, P. J.; Sarker, D. K.; Clark, D. C., Dynamic Surface Tension and Adsorption Properties of B-Casein and B-Lactoglobulin. *Food Hydrocolloids* **1996**, *10*, 395-405.

42. Cicuta, P.; Hopkinson, I., Studies of a Weak Polyampholyte at the Air–Buffer Interface: The Effect of Varying Ph and Ionic Strength. *The Journal of Chemical Physics* **2001**, *114*, 8659-8670.

43. Atkinson, P. J.; Dickinson, E.; Horne, D. S.; Richardson, R. M., Neutron Reflectivity of Adsorbed [Small Beta]-Casein and [Small Beta]-Lactoglobulin at the Air/Water Interface. *Journal of the Chemical Society, Faraday Transactions* **1995**, *91*, 2847-2854.

44. Maldonado-Valderrama, J.; Fainerman, V. B.; Galvez-Ruiz, M. J.; Martin-Rodriguez, A.; Cabrerizo-Vilchez, M. A.; Miller, R., Dilatational Rheology of Beta-Casein Adsorbed Layers at Liquid-Fluid Interfaces. *J. Phys. Chem. B* **2005**, *109*, 17608-17616.

45. Dickinson, E.; Horne, D. S.; Phipps, J. S.; Richardson, R. M., A Neutron Reflectivity Study of the Adsorption Of .Beta.-Casein at Fluid Interfaces. *Langmuir : the ACS journal of surfaces and colloids* **1993**, *9*, 242-248.

46. Ortega, F.; Ritacco, H.; Rubio, R. G., Interfacial Microrheology: Particle Tracking and Related Techniques. *Current Opinion in Colloid & Interface Science* **2010**, *15*, 237-245.

47. Davis, J. P.; Foegeding, E. A., Comparisons of the Foaming and Interfacial Properties of Whey Protein Isolate and Egg White Proteins. *Colloid Surf. B-Biointerfaces* **2007**, *54*, 200-210.

48. Dan, A., Interfacial Adsorption and Rheological Behavior of B-Casein at the Water/Hexane Interface at Different Ph. *Food hydrocolloids* **2014**, *v. 34*, pp. 193-201-2014 v.34.

49. Lee, M. H.; Reich, D. H.; Stebe, K. J.; Leheny, R. L., Combined Passive and Active Microrheology Study of Protein-Layer Formation at an Air−Water Interface. *Langmuir : the ACS journal of surfaces and colloids* **2010**, *26*, 2650-2658.

50. Cicuta, P., Compression and Shear Surface Rheology in Spread Layers of B-Casein and B-Lactoglobulin. *J. Colloid Interface Sci.* **2007**, *308*, 93-99.